Original article

VIDEO AVAILABLE ONLINE

# Optical scanning for rapid intraoperative diagnosis of sentinel node metastases in breast cancer

**M. R. S. Keshtgar[1], D. W. Chicken[1,2], M. R. Austwick[2], S. K. Somasundaram[1,2], C. A. Mosse[2], Y. Zhu[2,3], I. J. Bigio[4] and S. G. Bown[2]**

[1]Department of Surgery, [2]National Medical Laser Centre and [3]Department of Statistical Science, Royal Free and University College Medical School, University College London, London, UK, and [4]Departments of Biomedical Engineering and Electrical Engineering, Boston University, Boston, Massachusetts, USA

*Correspondence to:* Mr M. R. S. Keshtgar, Department of Breast Surgery, Royal Free Hospital, Pond Street, London NW3 2QG, UK (e-mail: m.keshtgar@ucl.ac.uk)

**Background:** **Intraoperative diagnosis of sentinel node metastases enables an immediate decision to proceed to axillary lymph node dissection, avoiding a second operation in node-positive women with breast cancer.**

**Methods:** **An optical scanner was developed that interrogated the cut surface of bivalved, but otherwise unprocessed, sentinel lymph nodes with pulses of white light by elastic scattering spectroscopy (ESS). The scattered light underwent spectral analysis, and individual spectra were initially correlated with conventional histology to develop a diagnostic algorithm. This algorithm was used to create false colour-coded maps of scans from an independent set of nodes, and the optimal criteria for discriminating between normal and cancer spectra were defined statistically.**

**Results:** **The discriminant algorithm was developed from a training set of 2989 spectra obtained from 30 metastatic and 331 normal nodes. Subsequent scans from 129 independent nodes were analysed. The scanner detected macrometastases (larger than 2 mm) with a sensitivity of 76 per cent (69 per cent including micrometastases) and specificity of 96 per cent.**

**Conclusion:** **In this proof-of-principle study, the ESS results were comparable with current intraoperative diagnostic techniques of lymph node assessment.**

Paper accepted 24 February 2010

Published online 30 June 2010 in Wiley InterScience (www.bjs.co.uk). **DOI:** 10.1002/bjs.7095

## Introduction

Sentinel lymph node biopsy (SLNB) has been validated as an accurate technique for axillary lymph node staging in breast cancer. Five randomized controlled trials have confirmed the accuracy and reduced morbidity compared with routine axillary lymph node dissection (ALND)[1–5]. Patients with tumour in the sentinel node may have further metastases in other axillary nodes. Current surgical practice in this situation is to proceed to ALND[6]. If analysis of the node cannot be undertaken during surgery, ALND will be required later in node-positive patients. ALND as a second operation is technically more difficult, delays the start of adjuvant radiotherapy and chemotherapy, has additional cost implications and may have an adverse psychological impact.

Conventional intraoperative analysis is undertaken by touch imprint cytology (TIC) or frozen-section histology. Both require sample preparation and interpretation of the findings by an experienced pathologist. The aim was to develop a potentially inexpensive device that could analyse nodes automatically during surgery with a minimum of tissue or slide preparation, and without the need for the availability of a histology technician, pathologist or cytologist for preparation and interpretation.

There is increasing interest in optical techniques for detection of cancer. Spectroscopic measurements enable *in vivo* or *ex vivo* examination and computer-generated diagnosis without tissue processing[7]. The present system for elastic scattering spectroscopy (ESS) interrogates tissue with short pulses of white light, recording the spectra of backscattered light and using statistical tools to

discriminate between spectra from normal and abnormal tissues. The system is sensitive to cellular and subcellular changes known to occur in malignancy[8], although the statistical methods reported here do not correlate directly spectra with specific physical properties of normal and malignant cells. ESS point measurements using a fibreoptic probe are able to distinguish between normal and metastatic lymph nodes[9,10]. The hypothesis studied here was that more comprehensive optical sampling of the tissue under examination should increase the accuracy of diagnosis.

This paper describes a novel prototype ESS scanning device that can optically interrogate the cut surface of an excised node within a few minutes, and give an immediate objective computer-generated diagnosis without the need for a pathologist's interpretation. This proof-of-principle study aimed to determine the accuracy of detection of clinically relevant sentinel node metastases compared with histopathological analysis of formalin-fixed tissue. The secondary aim was to compare ESS diagnosis with TIC, a widely used routine intraoperative diagnostic procedure. TIC was chosen over frozen-section analysis as TIC and ESS are both techniques for analysing the cut surface of a lymph node.

## Methods

### Elastic scattering spectroscopy system

The ESS system has been described previously[8,9]. Under control from a laptop computer, short pulses of white light from a xenon arc lamp (Perkin Elmer, Fremont, California, USA) are delivered to tissue via a 0·4-mm diameter fibre in contact with the target tissue. Scattered light for subsequent analysis is collected by a second fibre (0·2 mm) immediately adjacent to the first (approximately 0·32 mm centre-to-centre separation) (*Fig. 1*). The system compensates for background light and ensures that the detected light does not saturate the detector. All spectra are recorded as a ratio to a calibration spectrum taken from a spectrally flat material (Spectralon®; Labsphere, Cranfield, UK), thus rendering the data independent of the spectral response of the system.

### Study design

Ethics committee approval was obtained for this study. Patients with a preoperative diagnosis of breast cancer who did not have known involved axillary lymph nodes underwent SLNB using the combined technique of blue dye and radiocolloid for node localization[11]. At the time of this study, patients did not have routine axillary ultrasonography before surgery.

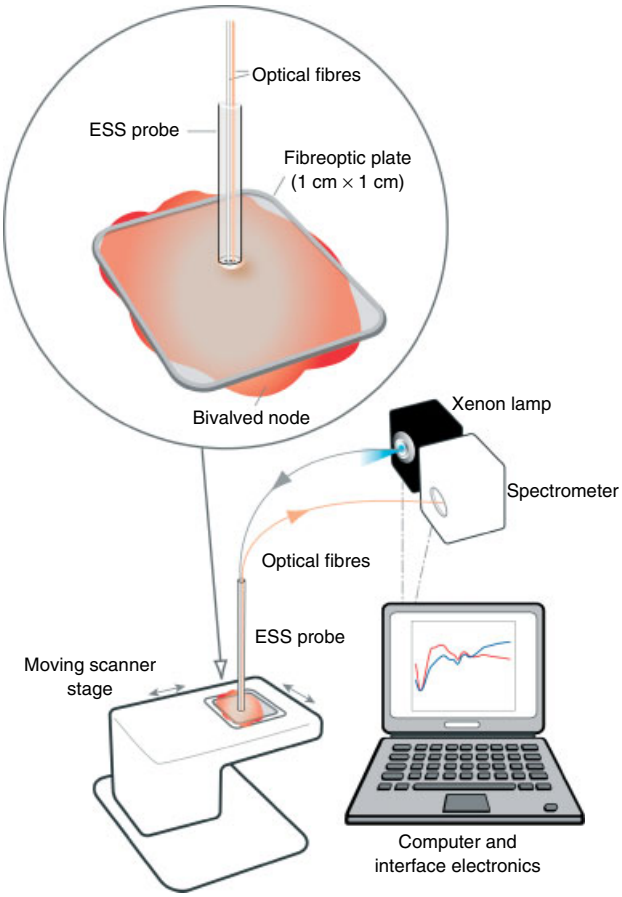


**Fig. 1** Schematic diagram of elastic scattering spectroscopy (ESS) system. The node is scanned through a fibreoptic plate by moving it on a stage under a fixed probe

After excision, nodes were bivalved along their long axis. TIC was performed by dabbing a coated glass slide on to the cut surface, drying and staining with a rapid May–Grunwald–Giemsa stain before examination by an expert cytologist, as described previously[12]. ESS measurements were then taken from the same cut surface of the node.

The study was conducted in two phases. Initially spectra from nodes subsequently shown to be entirely normal or replaced by cancer (at least 80 per cent of the surface replaced by cancer, identified macroscopically and confirmed histologically) were used to develop an algorithm to distinguish cancer from normal node tissue. Each spectrum was acquired by placing the optical probe manually at up to 16 random sites on the bivalved node. In the second phase, an independent set of nodes was scanned,

and the discriminant algorithm was used to generate a high-resolution map showing cancerous regions of the node.

## Scanner development

The difficulty with scanning a bivalved node is that the probe has to be in contact with the tissue at each measurement point. This problem was overcome by using a sprung plate to press the cut surface of the node lightly on to the underside of a fibreoptic plate (Hamamatsu Photonics, Hamamatsu, Japan). The fibres in each channel of the microchannel fibreoptic plate were much smaller than the probe's fibres (4 μm *versus* 0·2 and 0·4 mm) and so transmitted an image of the tissue on to the probe. The tissue and plate were then moved in a raster scanning pattern under a stationary ESS probe that was optically coupled to it by a drop of immersion oil (*Fig. 1*). The motorized scanner first used for this study moved slowly and an entire scan took 20 min. A newer version took 8 min and could be speeded up further by hardware modification. Before use, the system response was calibrated through the fibreoptic plate using the diffuse reflection standard material (Spectralon®). The scanner was set to collect 400 spectra at 0·5-mm intervals across a square centimetre. The scanner is simple to set up and can be used by an operating theatre technician after demonstration on a couple of nodes, while the surgeon is proceeding with excision of the primary cancer in the breast itself. A video of the ESS procedure may be found in *Appendix 1* (supporting information).

When optical measurements were complete and samples obtained for TIC, the bisected nodes were fixed in 10 per cent formalin and sent for routine histopathological analysis with multilayer sectioning (minimum three levels) and staining with haematoxylin and eosin. A fourth level was taken and sent for immunohistochemical staining. These results from routine histology were taken as the reference standard. Metastatic nodes were thereby subclassified as containing macrometastases (larger than 2 mm) or micrometastases (0·2–2 mm). According to current American Society of Clinical Oncology Technology Assessment Panel guidelines, completion ALND would not be undertaken for any deposit smaller than 0·2 mm or with isolated tumour cells detectable only by immunohistochemistry; therefore, for the purposes of this study such nodes were regarded as non-metastatic, although their presence was noted[11].

## Spectral and statistical analysis

The spectra were analysed using purely statistical techniques as reported previously[9]. In brief, the analysis consisted of smoothing, just using wavelengths in the visible and near-infrared part of the spectrum (400–800 nm), normalization and sevenfold data reduction (using only one in seven data points to leave just 87 data points per spectrum). This data reduction allowed each spectrum to be analysed within fractions of a second.

Principal component analysis is a standard statistical technique which extracts the features that vary between different spectra; features that do not significantly vary are disregarded, greatly reducing the size of the spectral data set. Analysis of the training data set (data used to develop the diagnostic algorithm) was undertaken using principal component analysis and then discriminating between classes by linear discriminant analysis on the first 20 principal components. A discriminant algorithm was developed by leave-one-out cross-validation of the training set of spectra. Linear discriminant analysis determines an axis along which the intergroup distance is largest compared with the group variances. In this way the groups (normal and metastatic) were separated optimally. Projecting the spectral values on to the axis of maximum separation gave the canonical score, a direct indicator of the group. The optical spectrum of the patent blue dye used to locate the sentinel node did not contribute to the variability[9].

For the second part of the study (testing the algorithm), a 10 × 10-mm area on the cut surface of nodes was scanned at 400 spectra per $cm^2$. The spectra from these scans constituted a test set of data entirely independent of those used for the training set and included spectra from nodes that were partially or completely replaced by cancer or were entirely normal. During the early measurements, two particular sources of instrumental artefact were identified and eliminated. Saturation of the optical detector (spectrometer) was prevented by a feedback system that limited the number of white light pulses used for each spectrum, and difficulty identifying the border of nodes was resolved by scanning the nodes against a green background. The previously developed discriminant algorithm was used to calculate the canonical score for each pixel within the 20 × 20 matrix. An image was generated by plotting the canonical scores as a false colour map.

The final step was to define conditions for labelling each node as metastatic or non-metastatic. A computer routine was written to determine the size of the maximum cluster of pixels (pixels contiguous with each other) exceeding canonical scores of 0·5, 1·0, 1·5, 2·0 and 2·5 in each scan. This was correlated with the final histology, and a receiver operating characteristic (ROC) curve was generated by varying the threshold minimum cluster size for diagnosis of metastases. A clump-based criterion is more robust against per-spectra false positives than simply counting the

number of positive pixels in the node; the likelihood of nine (the number found to be optimal) random false positives appearing in adjacent positions is much lower than that for nine scattered pixels occurring over a node.

The accuracy of diagnosis of sentinel node metastases was determined by comparing the diagnosis made by ESS scanning with that on histopathology. A further analysis compared the sensitivity of ESS diagnosis with that of TIC in relation to the final histopathology result. These analyses were performed on a per-node basis.

## Results

### Algorithm development

The diagnostic algorithm was developed from 2989 technically satisfactory ESS spectra (spectra without saturation of the spectrometer) from 331 normal and 30 metastatic nodes. Approximately equal numbers of spectra were taken from each node. The means of the cropped, smoothed and normalized spectra for normal and metastatic tissues in the training set are shown in *Fig. 2*. *Fig. 3* shows the distribution of canonical scores of spectra from normal and metastatic nodes in the training data set. For the spectra from metastatic nodes, there were two dominant peaks, the first at a score of 0, corresponding to the single peak seen from normal nodes, and a second at 4, seen only with metastatic nodes. This multimodal distribution with metastatic nodes suggests that, despite the selection of spectra from known areas of cancer for training, there remained a mix of normal and metastatic spectra, presumably related to remaining normal structures within the metastatic nodes.

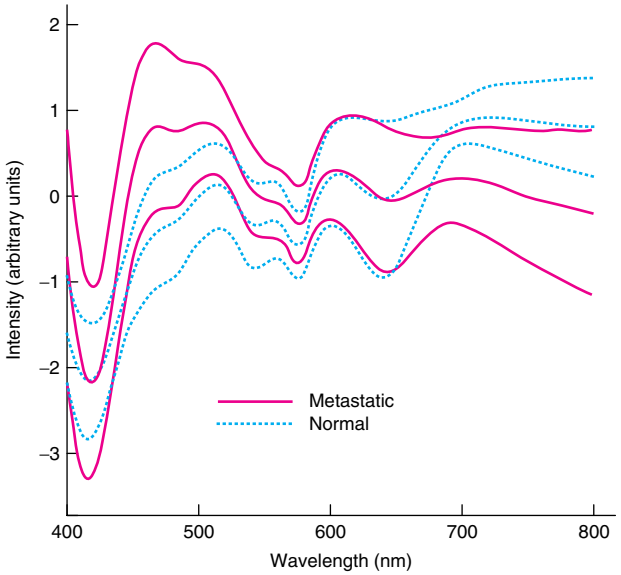


**Fig. 2** Mean cropped, smoothed and normalized spectra from 331 normal nodes and 30 metastatic nodes, with standard deviations

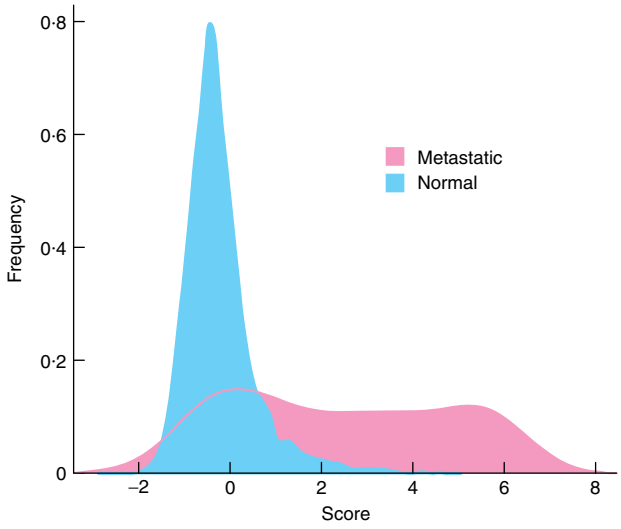


**Fig. 3** Distribution plot of canonical scores of spectra from the training data set determined by linear discriminant analysis using 20 principal components. The frequency is plotted as a percentage of class

### Scanner results

The diagnostic algorithm was tested on an independent set of 129 nodes with technically satisfactory scans (spectra without saturation of the spectrometer and with good definition of the position of the edge of the node). These 129 nodes comprised 45 with macrometastases, seven with micrometastases, three with submicrometastases or isolated tumour cells and 74 normal nodes as determined by standard histology. A representative scan of a node containing a metastasis is shown in *Fig. 4a*. *Table 1* shows the sensitivity for detection of metastases for each subclass. Thirty-four of 45 nodes that contained macrometastases were detected by ESS, but only two of seven with micrometastases. For the 91 nodes in this series that were also assessed by TIC, the results are compared in *Table 2*.

ROC curves were plotted for canonical scores of 0·5, 1·0, 1·5, 2·0 and 2·5 (*Fig. 5*). The greatest accuracy (area under the curve) was achieved with a canonical score threshold for cancer diagnosis of 2·0; an optimal balance of sensitivity and specificity was found for a minimum clump size of nine positive pixels. This gave an overall specificity of 96 per cent and sensitivity of 69 per cent for the detection of cancer. The incidence of sentinel node metastases in the

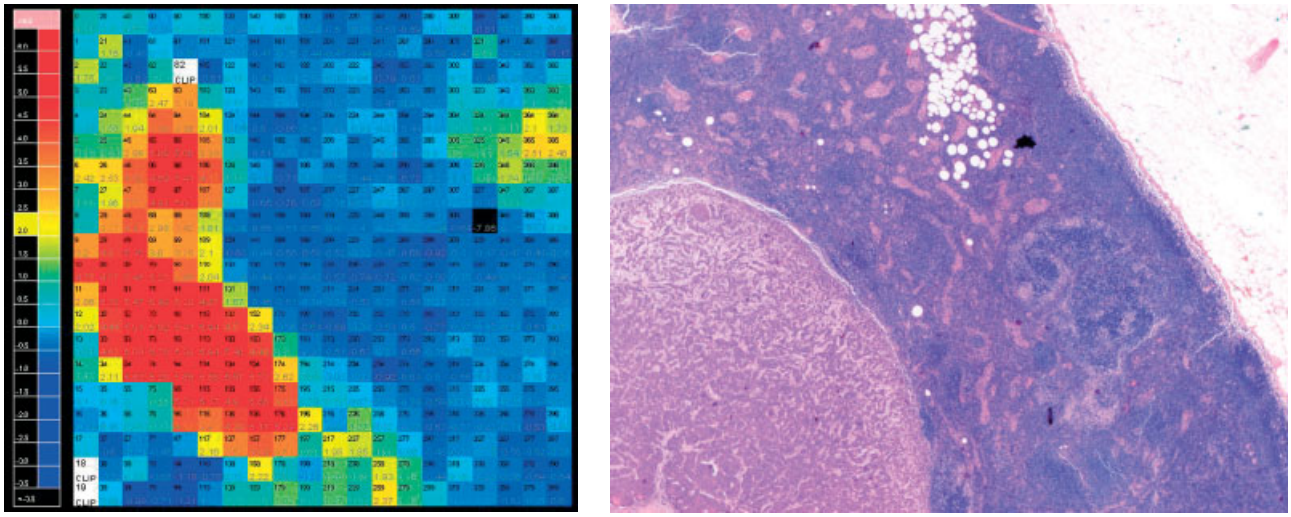

**a** False colour-coded scan **b** Histology

**Fig. 4** **a** False colour-coded scan of a node showing a single metastasis in the left lower quadrant. Colours are based on the canonical score for each pixel from blue (low score, indicates normal node) to red (high score, indicates metastasis). The cut-off chosen to discriminate between normal and cancer for individual pixels (canonical score 2) is where the colour changes from pale green to yellow. **b** Histology image showing the junction of a metastasis (lower left) with normal lymphatic tissue (upper right) (haematoxylin and eosin stain, original magnification ×400)

**Table 1** Sensitivity of detection of axillary lymph node metastases using elastic scattering spectroscopy by histological subclass

| Histological subclass | No. of Nodes | True positive | False positive | True negative | False Negative | Sensitivity (%) |
|---|---|---|---|---|---|---|
| Macrometastases > 2 mm | 45 | 34 | 0 | 0 | 11 | 76 |
| Micrometastases 0·2–2 mm | 7 | 2 | 0 | 0 | 5 | 29 |
| Submicrometastases < 0·2 mm and ITCs | 3 | 0 | 0 | Non-metastatic | 0 | 0 |
| Normal | 74 | 0 | 3 | 71 | 0 | – |

Nodes with submicrometastases and isolated tumour cells (ITCs) on histology were regarded as non-metastatic.

**Table 2** Comparison of sensitivity and specificity of elastic scattering spectroscopy and touch imprint cytology for detection of sentinel node metastases in the subset of 91 nodes that underwent both procedures

| | | ESS | | TIC | |
|---|---|---|---|---|---|
| Histological subclass | No. of nodes | True positive* | False positive† | True positive* | False positive† |
| Macrometastases > 2 mm | 26 | 18 (69) | | 23 (88) | |
| Micrometastases 0·2–2 mm | 5 | 2 (40) | | 0 (0) | |
| Submicrometastases < 0·2 mm and ITCs | 3 | 0 (0) | | 0 (0) | |
| Normal | 57 | | 2 (97) | | 0 (100) |

Values in parentheses are *sensitivity (%) and †specificity (%). ESS, elastic scattering spectroscopy; ITC, isolated tumour cell; TIC, touch imprint cytology.

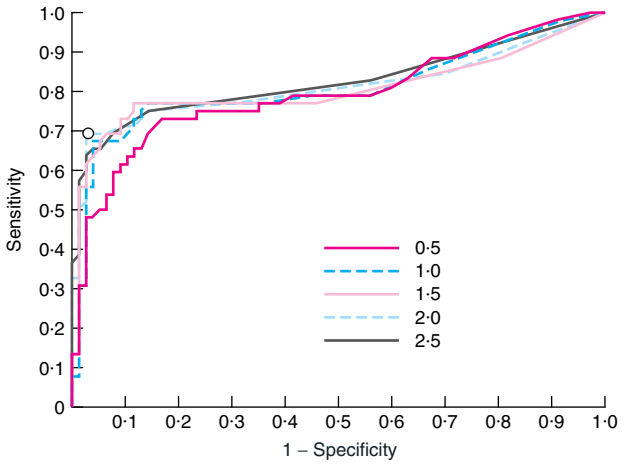


**Fig. 5** Receiver operating characteristic (ROC) curves showing sensitivity *versus* false-positive rate (1 − specificity), generated by varying the threshold canonical score (from 0·5 to 2·5) and threshold number of pixels in a cluster. Along each curve, the number of pixels in the cluster increases from right to left. The point chosen as the optimum is circled, with a cluster size of 9 and a canonical score of 2·0

population of women undergoing breast cancer surgery is approximately 30 per cent[3], giving a positive predictive value of 88 per cent and a negative predictive value of 88 per cent.

## Discussion

The standard of care in centres practising intraoperative analysis of the sentinel node in patients with early breast cancer is to identify and excise the sentinel node(s), then proceed to excise the primary breast tumour, while the excised node is being tested for cancer. This typically gives a window of 30–40 min for examination of the node. If cancer is detected, the surgeon can perform ALND during the same operation, as required for optimal local control and staging of the disease.

The current routine techniques for immediate assessment of excised sentinel nodes are TIC and frozen-section histology, both of which have close to 100 per cent specificity, although variable sensitivity (23–100 per cent). The results depend mainly on the completeness of sampling and the skill of the pathologist[12–14]. Both require tissue processing and the immediate availability of a pathologist to interpret the findings. Many centres are unable to offer this service owing to the practical difficulties of preparing and examining the specimen urgently, even if remote image viewing is available.

The present pilot study suggests that ESS is a potential alternative technique for the immediate detection of cancer in excised sentinel nodes. As would be expected, the best results (76 per cent sensitivity) were with macrometastases (larger than 2 mm). Even so, sensitivity was limited as only a single 10 × 10-mm area of one cut surface of each node was scanned in this study. Many of the nodes had a surface area greater than this. Furthermore, as ESS interrogates tissue only to a depth of about 0·5 mm[9], comprehensive scanning would require cutting a node into 1-mm slices and then scanning both sides of every slice. Small metastatic deposits are often found in the subcapsular area of the node, so could easily be missed by a scan that covered only the centre of a large node. Using the latest prototype equipment, each scan takes about 8 min, but future engineering improvements should be able to reduce this significantly and make it realistic to scan several surfaces larger than 1 $cm^2$ within the typical timespan available of 30–40 min.

Only two of seven nodes with micrometastases (0·2–2 mm) were detected by ESS. This is not surprising as nine contiguous pixels were required to have spectra with canonical scores above the threshold to make a diagnosis of cancer. With the scanner moving 0·5 mm between pixels, the midpoint of nine pixels is 0·7 mm from the centre of the outer pixels. Thus if cancer cannot be detected more than 0·5 mm from a probe position, the smallest cancer deposit that would be detectable would be 0·4 mm across, and then only if it was in exactly the right place in relation to the pixel locations. This problem could be addressed by rescanning, either at the same resolution (looking for correlation between positive pixels between the two scans when there were fewer than nine contiguous positive pixels) or at higher spatial resolution, focusing on suspicious areas.

TIC detected more macrometastases than ESS (23 compared with 18), most likely because the imprint was taken from the whole cut surface of nodes, which in many cases was considerably larger than the 1 $cm^2$ scanned by ESS. In contrast, TIC did not detect any micrometastases, whereas ESS detected two of the five nodes in this category. This is probably because the micrometastases were located just below the cut surface that was imprinted. One of the key attractions of ESS is that the results do not depend on the availability of a pathologist or cytologist.

Improving the sensitivity is important, but specificity is paramount to avoid the risk of proceeding with ALND in a patient who does not need it; all patients undergoing ALND are at risk of lymphoedema and shoulder dysfunction[11]. There were three false positives among the 74 normal nodes in the present series of 129 nodes. It was not possible to identify any clinical, pathological or technical factors to account for these

findings but it could be anticipated that, as the database on which the diagnostic algorithm is based increases in size and scanning techniques and statistical analyses are refined further, the number of false positives will fall and the sensitivity will rise. A faster scanner would enable rapid rescanning of nodes at different pixel separations. If the scans are reproducible, this may help clarify questionable results, as well as indicating whether metastases are present or not in suspicious areas.

Rapid polymerase chain reaction assay is another technique currently under assessment for detecting cancer in excised axillary nodes without requiring a pathologist to interpret the findings[15,16]. These can give a result in a time comparable to ESS, but there are several disadvantages. The equipment is more complex and less convenient for use in or close to the operating theatre, staff require several days of training to be able to operate it, and the running costs are higher than for ESS. In addition, as tissue has to be homogenized to undertake the analysis, it would not be suitable for standard histological examination (although part of the node could be saved for formal histology). The molecular approach gives no indication of the size of any cancer deposit detected, so cannot discriminate between deposits that do and do not require ALND.

During this preliminary study of ESS scanning, several instrumental, experimental and analytical problems were identified and addressed. It is clear that further refinements are needed before this technology is ready for routine clinical use, but in principle ESS scanning is capable of rapidly detecting metastases within sentinel nodes with a clinically useful sensitivity and specificity using current prototype equipment. This needs validation in a multicentre trial when the equipment and analytical techniques have been optimized. The system potentially has wider applications. ESS point measurements are able to detect dysplasia and early cancer *in vivo* in Barrett's oesophagus[17], dysplastic polyps in the colon[18] and dysplasia in oral mucosa[19]. The ESS scanning method described in this paper is an important advance on point measurements, as it examines a larger area of tissue and can produce high-resolution diagnostic images of any tissue that can be optically scanned. As the computer makes the diagnosis, the technique could be used in any hospital, enabling similar sensitivity and specificity of diagnosis to that obtained using conventional techniques in specialist centres.

## Acknowledgements

The authors acknowledge important contributions to this work from the following individuals: Benjamin Clark and Kristie Johnson for early work on the analytical routines and technical and software development, Gabrijela Kocjan and Mary Falzon for expert histopathological and cytological analysis, Tom Fearn for development of statistical techniques, and Richard Sainsbury and Michael Douek for help with recruitment of patients for the study.

Research funding came from the United States Department of Defense Breast Imaging Program (award number W81XWH-04-1-0589) and from Hamamatsu Photonics (Hamamatsu, Japan). This work was developed in part as an extension to the authors' participation in the National Institutes of Health programme 'Network on Translational Research on Optical Imaging (NTROI)' (U54 CA104677). The work was undertaken at University College London Hospital and University College London, which received a proportion of funding from the Department of Health's National Institute for Health Research Biomedical Research Centres funding scheme. The authors declare no conflict of interest.

## References

1 Veronesi U, Paganelli G, Viale G, Luini A, Zurrida S, Galimberti V *et al.* A randomized comparison of sentinel-node biopsy with routine axillary dissection in breast cancer. *N Engl J Med* 2003; **349**: 546–553.
2 Purushotham AD, Upponi S, Klevesath MB, Bobrow L, Millar K, Miles J *et al.* Morbidity after sentinel lymph node biopsy in primary breast cancer: results from a randomized controlled trial. *J Clin Oncol* 2005; **23**: 4312–4321.
3 Mansel RE, Fallowfield L, Kissin M, Goyal A, Newcombe RG, Dixon JM *et al.* Randomized multicenter trial of sentinel node biopsy *versus* standard axillary treatment in operable breast cancer: the ALMANAC Trial. *J Natl Cancer Inst* 2006; **98**: 599–609.
4 Del Bianco P, Zavagno G, Burelli P, Scalco G, Barutta L, Carraro P *et al.* Morbidity comparison of sentinel lymph node biopsy *versus* conventional axillary lymph node dissection for breast cancer patients: results of the sentinella-GIVOM Italian randomised clinical trial. *Eur J Surg Oncol* 2008; **34**: 508–513.
5 Gill G; SNAC Trial Group of the Royal Australasian College of Surgeons (RACS) and NHMRC Clinical Trials Centre. Sentinel-lymph-node-based management or routine axillary clearance? One-year outcomes of sentinel node biopsy *versus* axillary clearance (SNAC): a randomized controlled surgical trial. *Ann Surg Oncol* 2009; **16**: 266–275.
6 Keshtgar MR, Ell PJ. Clinical role of sentinel-lymph-node biopsy in breast cancer. *Lancet Oncol* 2002; **3**: 105–110.
7 Bigio IJ, Bown SG. Spectroscopic sensing of cancer and cancer therapy: current status of translational research. *Cancer Biol Ther* 2004; **3**: 259–267.
8 Mourant JR, Canpolat M, Brocker C, Esponda-Ramos O, Johnson TM, Matanock A *et al.* Light scattering from cells:

the contribution of the nucleus and the effects of proliferative status. *J Biomed Opt* 2000; **5**: 131–137.
9 Johnson KS, Chicken DW, Pickard DC, Lee AC, Briggs G, Falzon M *et al*. Elastic scattering spectroscopy for intraoperative determination of sentinel lymph node status in the breast. *J Biomed Opt* 2004; **9**: 1122–1128.
10 Bigio IJ, Bown SG, Briggs G, Kelley C, Lakhani S, Pickard D *et al*. Diagnosis of breast cancer using elastic-scattering spectroscopy: preliminary clinical results. *J Biomed Opt* 2000; **5**: 221–228.
11 Lyman GH, Giuliano AE, Somerfield MR, Benson AB III, Bodurka DC, Burstein HJ *et al*. American Society of Clinical Oncology guideline recommendations for sentinel lymph node biopsy in early-stage breast cancer. *J Clin Oncol* 2005; **23**: 7703–7720.
12 Chicken DW, Kocjan G, Falzon M, Lee AC, Douek M, Sainsbury R *et al*. Intraoperative touch imprint cytology for the diagnosis of sentinel lymph node metastases in breast cancer. *Br J Surg* 2006; **93**: 572–576.
13 Tew K, Irwig L, Mathews A, Crowe P, Macaskill P. Meta-analysis of sentinel node imprint cytology in breast cancer. *Br J Surg* 2005; **92**: 1068–1080.
14 Veronesi U, Zurrida S, Mazzarol G, Viale G. Extensive frozen section examination of axillary sentinel nodes to determine selective axillary dissection. *World J Surg* 2001; **25**: 806–808.
15 Julian TB, Blumencranz P, Deck K, Whitworth P, Berry DA, Berry SM *et al*. Novel intraoperative molecular test for sentinel node metastases in patients with early-stage breast cancer. *J Clin Oncol* 2008; **26**: 3338–3345.
16 Visser M, Jiwa M, Horstman A, Brink AA, Pol RP, van Diest P *et al*. Intra-operative rapid diagnostic method based on CK19 mRNA expression for the detection of lymph node metastases in breast cancer. *Int J Cancer* 2008; **122**: 2562–2567.
17 Lovat LB, Johnson K, Mackenzie GD, Clark BR, Novelli MR, Davies S *et al*. Elastic scattering spectroscopy accurately detects high grade dysplasia and cancer in Barrett's oesophagus. *Gut* 2006; **55**: 1078–1083.
18 Dhar A, Johnson KS, Novelli MR, Bown SG, Bigio IJ, Lovat LB *et al*. Elastic scattering spectroscopy for the diagnosis of colonic lesions: initial results of a novel optical biopsy technique. *Gastrointest Endosc* 2006; **63**: 257–261.
19 Sharwani A, Jerjes W, Salih V, Swinson B, Bigio IJ, El Maaytah M *et al*. Assessment of oral premalignancy using elastic scattering spectroscopy. *Oral Oncol* 2006; **42**: 343–349.

## Supporting information

Additional supporting information may be found in the online version of this article.

**Appendix 1** Video of the elastic scattering spectroscopy procedure in breast cancer

Please note: John Wiley & Sons Ltd is not responsible for the content or functionality of any supporting materials supplied by the authors. Any queries (other than missing material) should be directed to the corresponding author for the article.